

# Fluorescence lifetime imaging microscopy in the medical sciences

René Ebrecht · Craig Don Paul · Fred S. Wouters

Received: 4 December 2013 / Accepted: 12 December 2013 / Published online: 4 January 2014  
© Springer-Verlag Wien 2014

**Abstract** The steady improvement in the imaging of cellular processes in living tissue over the last 10–15 years through the use of various fluorophores including organic dyes, fluorescent proteins and quantum dots, has made observing biological events common practice. Advances in imaging and recording technology have made it possible to exploit a fluorophore's fluorescence lifetime. The fluorescence lifetime is an intrinsic parameter that is unique for each fluorophore, and that is highly sensitive to its immediate environment and/or the photophysical coupling to other fluorophores by the phenomenon Förster resonance energy transfer (FRET). The fluorescence lifetime has become an important tool in the construction of optical bioassays for various cellular activities and reactions. The measurement of the fluorescence lifetime is possible in two formats; time domain or frequency domain, each with their own advantages. Fluorescence lifetime imaging applications have now progressed to a state where, besides their utility in cell biological research, they can be employed as clinical diagnostic tools. This review highlights the multitude of fluorophores, techniques and clinical applications that make use of fluorescence lifetime imaging microscopy (FLIM).

**Keywords** Organic dyes · Quantum dots (QDs) · Fluorescent proteins (FPs) · Quenchers · Förster resonance energy transfer (FRET) · Fluorescence lifetime imaging microscopy (FLIM) · Time-domain FLIM (TD FLIM) · Frequency-domain FLIM (FD FLIM) · Endogenous fluorophores

Handling Editor: J. W. Borst

R. Ebrecht · C. Don Paul (✉) · F. S. Wouters  
Department of Neuro- and Sensory Physiology, University Medicine  
Göttingen, 37073 Göttingen, Germany  
e-mail: craig.donpaul@med.uni-goettingen.de

R. Ebrecht · C. Don Paul · F. S. Wouters  
Center for Nanoscale Microscopy and Molecular Physiology of the  
Brain (CNMPB), Göttingen, Germany

## Introduction

In the quest to improve our knowledge of the cell and its inner workings, a detailed picture of signalling events is required. Traditional biochemical analytical techniques allow identifying individual molecular components of biochemical pathways, but this is mostly accomplished by disruption of the cell. Therefore, fluorescence imaging has become essential by its non-invasive approach in deducing biomolecular details of specific signaling pathways in living cells. Subsequently, fluorescent labelling of molecules of interest has become, over its many decades of use, the primary method for cellular imaging in the life sciences (Lakowicz 2006).

Ideally, as we wish to learn about fast biological events at minute concentrations, the fluorescent labels to be used must be fast, photostable and bright in order to detect infrequent biological events (Resch-Genger et al. 2008). A fluorescent probe that possesses these qualities, however, does not make it always ideal for use in biology. Besides its spectral qualities, the ideal biological reporter fluorophore must be biocompatible, relatively non-toxic and stable under illumination at various pH and ion concentrations. Advantageously for using fluorescent labels in biological samples, compared to radioactive labels, is the utilisation of multiple fluorescent labels in the same sample at the same time, as long as their spectra are resolvable (Resch-Genger et al. 2008; Walling et al. 2009).

In general, fluorophores are characterised by their excitation and emission spectrum, and their governing parameters, the extinction coefficient — the ability to absorb light relative to its concentration as given by Lambert–Beer's law — and quantum yield — the efficiency with which absorbed photons are re-emitted as fluorescence. The product of these properties defines the brightness of a fluorophore. The basic principle of fluorescence can be visualised in a Jablonski diagram, in which the energetic states of the fluorophore under illumination is displayed (Fig. 1). Light absorption by the fluorophore (excitation) brings it

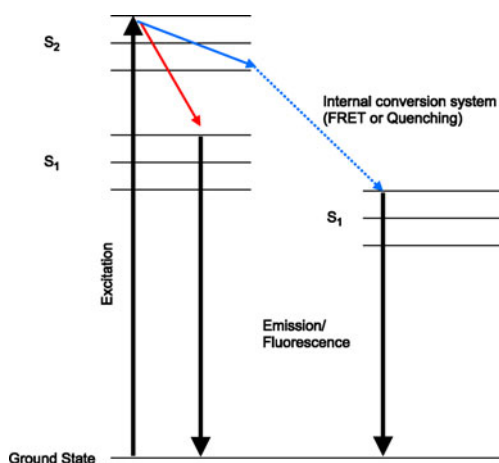


**Fig. 1** Absorption of a photon raises a ground state electron to a higher energy state ( $S_2$ ). Energy losses occur either within the fluorophore (red arrow) or through internal conversion systems to an additional fluorophore (blue arrows) to a lower energy level ( $S_1$ ). Upon its return to the ground state, the electron emits a photon, which can be detected as fluorescence

into an excited state. Upon decay to the ground state by emitting a photon (fluorescence), the energy of this photon is less compared to the excitation energy, which is due to vibrational relaxation, and results in a red shift of the emission colour (Stokes shift). In addition to these transitions that give rise to the typical fluorescence cycle, alternate sources for energy losses can occur, often to another fluorophore or quencher, discussed later in this review. The interplay of these transitions defines an additional descriptive property of the fluorescence process: the fluorophore lifetime — the time the fluorophore spends in the excited state prior to returning to the ground state. This parameter is inherent to all fluorophores and is highly sensitive to the fluorophore's molecular structure and its environment. Rarely exploited in cellular imaging, fluorescence lifetime measurements permit precise recording of the fluorophores immediate environment (Lakowicz 2006).

Autofluorescence from naturally fluorescent molecules within the cell, tissue or medium can be a confounding condition for the detection of fluorophores in biological imaging. Examples of naturally occurring fluorescent molecules include nicotinamide adenine dinucleotide (NAD), flavin adenine dinucleotide (FAD), melanin, FMN or riboflavin and the aromatic residues in proteins, which can all contribute to autofluorescence. As their emission mainly occur in the low-wavelength side of the visible optical spectrum, fluorophores whose emission is red (600–700 nm) or higher in the near-infrared (NIR) (>700 nm) spectrum are often more useful (Lakowicz 2006).

Today, there exists a large collection of fluorophores in various classes including organic dyes, luminescent nanoparticles like quantum dots (QDs) and fluorescent proteins (FPs), from which one can be selected with the desired fluorescence properties required for a particular imaging experiment (Lakowicz

2006; Resch-Genger et al. 2008). With the high sensitivity of fluorescence detection, the biological environment or labelled components can be interrogated through various assays (Becker 2012).

## Organic dyes and immunofluorescence

Organic dyes span the entire visible spectrum and even into the NIR spectrum (Resch-Genger et al. 2008; Terai and Nagano 2013). As they have been utilised for many years in various imaging techniques, a multitude of well-characterised dyes are commercially available. These dyes possess excellent water solubility and permit their facile covalent attachment to various side groups of proteins (amino-, carboxy, thiol, azide, etc.) by appropriate chemistry (Waggoner 2006; Resch-Genger et al. 2008). Advantageously, their small size minimises steric hindrance of the fluorophore label, permitting binding of several dye molecules to a biomolecule of choice. However, very high degrees-of-labelling is often accompanied by undesired fluorescence quenching or target malfunction (Resch-Genger et al. 2008).

Organic dyes can be divided into two categories: resonance or charge transfer dyes. Resonance dyes are characterised by structured, narrow and mirrored absorption/emission profiles, small Stokes shifts, high extinction coefficients and quantum yields. Charge transfer dyes on the other hand, although showing lower extinction coefficients and quantum yields, have well-separated, broader profiles and structureless absorption/emission profiles with large Stokes shifts (Resch-Genger et al. 2008). The lower brightness of these dyes is balanced by the increased separation in their spectral detection characteristics.

The specificity of an organic-based dye can be maximised through its conjugation to an antibody. Modern use of organic dyes has moved beyond the classical histological staining of broad substance classes and has moved from a 'tinctorial' to a 'targeted' staining mode. Immunofluorescence utilises the specificity of an antibodies' binding domain to target a dye to a particular protein or unique protein epitope.

Organic dyes, conjugated to antibodies, have the advantage of being applicable in imaging experiments ranging from individual cells to tissue slices. Utilising either primary or secondary immunofluorescence markers, labelling a protein of interest can be achieved. As immunolabelling is primarily used in fixed cells and tissues, their use in cell biology is restricted to the detection of static localisations. Indirect immunofluorescence assays can be used to detect various biological states. In the last few years, this limitation was lifted by the use of genetically encoded binding sites for organic dyes that can be incorporated in proteins of use, and can be expressed in the target tissues (Bunt and Wouters 2004).

## Quantum dots

Nanosized semiconductor crystals were found to possess bright and photostable fluorescence properties. These QDs were quickly exploited as fluorophores in bioimaging applications (Bruchez 2011). Spectrally, QDs are characterised by broad absorption spectra — providing multiple excitation options, and narrow emission spectra — permitting highly defined and precise detection (Walling et al. 2009). The narrow emission spectra of QDs results from the semiconductor shell forcing a narrow emission from the core, which enhances fluorescence brightness but reduces photobleaching (Walling et al. 2009). As a result, the fluorescence emission of QDs is tunable and depends on the particle or semiconductor size (Resch-Genger et al. 2008). Relative to organic dyes like rhodamine, QDs are approximately 20-fold brighter, 100-fold more photostable and occupy only one-third of the spectral width of the fluorescence emission profile (Chan and Nie 1998).

Notwithstanding their near-ideal spectral properties, prior to the employment of QDs in imaging experiments, some consideration must be made pertaining to the blinking, solvency and size of the QDs in use. The blinking of QDs, which can be disadvantageous during single-particle tracking experiments, can be averted through increasing the shell size or decreasing the excitation intensity during imaging (Chan and Nie 1998; Cui et al. 2007). As the shell of all QDs are comprised of inorganic materials, various coatings must be applied through various techniques (Chan and Nie 1998; Parak et al. 2002; Dubertret et al. 2002; Nann 2005; Gussin et al. 2006; Wang et al. 2007; Resch-Genger et al. 2008). As such, the final size of QDs vary greatly depending on its core material and the surface chemistry (Resch-Genger et al. 2008) and as the production of QDs depend on its purpose, there is no fixed protocol for surface conjugation of the multitude of possible surface additions in QDs (Xing et al. 2007). An unfortunate side effect of making QDs soluble is that their size can vary greatly, from small QDs approximately 1–6 nm, similar in size to most proteins, ranging up to 25 nm, depending on the coating or targeting sequences added (Åkerman et al. 2002; Chen and Gerion 2004; Resch-Genger et al. 2008). Although not being able to permeate the cell membrane, it is possible to introduce QDs inside cells through non-specific/receptor mediated endocytosis (Mitchell et al. 1999; Xing et al. 2007; Resch-Genger et al. 2008). In order to measure cell motility, QDs have also been utilised outside a cell with movement across a QD-matrix labelling motile cells and 'highlighting' areas of movement (Pellegrino et al. 2003).

In most cases, the semiconductor core of QDs is made from CdSe with a ZnS coating (Resch-Genger et al. 2008). Cytotoxicity, as a result of heavy metal 'poisoning' through possible Cd leakage from the QD has been observed in some cases (Parak et al. 2005; Resch-Genger et al. 2008); however,

other studies showed no cytotoxic effects of QDs (Chen and Gerion 2004). Either way, there is a push for cadmium free QDs, substituting the Cd shell with InGaP, InP or CuInS, due to the many restrictions that are currently in place with the use of heavy metals world wide (Pons et al. 2010; Mandal et al. 2013).

## Fluorescent proteins

Reportedly as early as the first century, Pliny the Elder observed the slime of the jellyfish (presumed to be *Pelagia noctiluca*) to glow in a way reminiscent of fire (Cubitt et al. 1995). Since the initial discovery, cloning and analysis of *Aequoria victoria* green fluorescent protein (GFP) (Shimomura et al. 1962; Chalfie et al. 1994; Tsien 1998), members of the GFP super-family have become indispensable tools in molecular biological imaging (Patterson et al. 1997; Tsien 1998). Originally purified as a green emissive protein, initial studies proved it possible to engineer colour variants that exhibited blue and yellow fluorescence emission (Cubitt et al. 1995). Since then, extensive work has generated colours spanning the entire visible spectrum from 400 to 650 nm (Matz et al. 1999; Kikuchi et al. 2008). Early work focused on improving their expression and photostability levels and therefore, current utilisation of FPs is relatively easy as they are highly efficient with well-characterised optical properties. There is a multitude of FPs currently available with a wide range of spectral and optical properties, with many available either commercially or on request (McNamara and Boswell 2008). Their fluorescence spectra, generally mirror images and separated by a small Stokes shift of approximately 10–20 nm make them suitable for many imaging techniques, including the imaging of multiple proteins/organelles in one experiment (Llopis et al. 1998; Shaner et al. 2005).

The use of FPs to monitor protein location was the first application in biological imaging (Chalfie et al. 1994). Their use in biology can be broadly categorised as to whether they are used for passive, active or interactive monitoring. The structure of FPs consists of an 11 stranded  $\beta$ -barrel and confers a high level of stability, which has been further enhanced to tolerate higher levels of 'environmental stress', including chemical, pH and photo-induced stress (Pédélecq et al. 2005; Don Paul et al. 2011, 2013). These proteins are most commonly utilised passively for monitoring protein localisation and trafficking, highlighted by their extensive use in biology. Interestingly, some proteins have been exploited for their lack of stability as the spectral properties of these FPs can be modulated through their interactions with their environment. These FPs have the ability to sense and report about their environment such as environmental pH (Abad et al. 2004) and metabolites (Miyawaki et al. 1997). Lastly, interactive FPs have the ability to interact with their

environment, such as KillerRed which produces reactive oxygen species upon illumination (Bulina et al. 2005; Vegh et al. 2011). FPs can also be utilised as biosensors of the cellular environment through either single FPs (Miesenböck et al. 1998) or via functional domains fused to the  $\beta$ -barrel (Griesbeck et al. 2001) making them capable of measuring small molecules. However, the most interesting category of biosensors are those relying on two FPs which can exploit the phenomenon of Förster resonance energy transfer (FRET). In the mid-1990s, the first biosensor based on FRET showed proteolysis activity by monitoring a loss of energy transfer between a blue and green FP (Mitra et al. 1996).

## Quenchers

Often, the ability to observe fluorescence is the only consideration that is made epitomised by choosing the brightest fluorophores. However, it must be noted that the ability to 'quench' fluorescence, thus modifying the original fluorescent signal, is also a very powerful imaging method. For example, the specificity and sensitivity of DNA primers used in reverse transcription-polymerase chain reaction (RT-PCR) experiments can be tested by using probes containing a fluorophore and quencher (Faltin et al. 2013). Fluorophore acceptors have the ability to receive excited energy from a nearby donor fluorophore. Subsequently, fluorescence from the acceptor is observed, which is also known as sensitised emission (Lakowicz 2006) and will be discussed later. Alternatively, if the acceptor is non-fluorescent, i.e., a quencher, the transferred energy will be dissipated into the surrounding environment as heat (Lakowicz 2006). Quenching can be achieved through various methods, the most common in molecular imaging techniques being via FRET (Lakowicz 2006). FRET quenching of the donor fluorophore will cause a measurable reduction of the donor fluorescence lifetime. Quenchers are currently available for most wavelengths in the visible spectrum and across all fluorophore classes. Coupled to various protein groups or even specific antibodies, quenchers can be used for measuring inter- or intra-molecular FRET (Gill and Le Ru 2011).

Quenching of QDs can be achieved through the addition of gold nanoparticles to their surface (Pons et al. 2007). Similar to organic dyes, quenching of FPs can be accomplished with other FPs or non-fluorescent FPs, known as chromoproteins. The first genetically encoded 'dark' quenchers, REACh1 and REACh2, were derived from EYFP to measure protein ubiquitination (Ganesan et al. 2006). Since then, various FP-based quenchers have been engineered including Ultramarine, an intensely blue coloured quencher for donors with emissions in the green to red range (Pettikiriachchi et al. 2012) and Phanta, an orange coloured quencher optimal for green emissive donors (Don Paul et al. 2013).

## FRET

First described by Theodore Förster over 60 years ago, FRET is a dipole–dipole interaction that occurs between two fluorophores that possess a spectral overlap between the donor's emission and acceptor's absorbance (Fig. 2a). It is important to note that the transfer of energy is non-radiative, i.e., it does not involve emission and re-absorption of photons (Förster 1948). The rate of energy transfer that occurs via FRET is described in the following equation (Lakowicz 2006):

$$K_{\text{FRET}} = \left(\frac{1}{\tau_{\text{D}}}\right) \left(\frac{R_0}{R}\right)^6$$

where  $\tau_{\text{D}}$  is the excited state lifetime of the donor and  $R$  is the distance separating the fluorophores. As the FRET critical distance ( $R_0$ ) between two fluorophores correlates inversely to the 6th power of separation distance, the FRET efficiency ( $E$ ) dramatically decreases with increasing distance in the vicinity of  $R_0$  (Fig. 2b) (Berney and Danuser 2003;

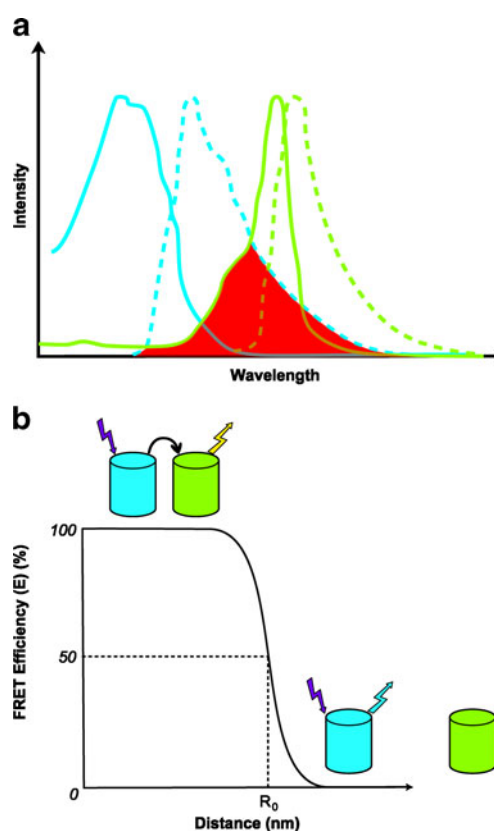


**Fig. 2** The CFP (cyan) and YFP (yellow) FRET-pair showing the excitation (solid line) and emission spectra (dashed line) (a). Highlighted (red) is the spectral overlap between CFP emission and YFP absorbance/excitation, a requirement for FRET. Highlighting the distant dependent nature of FRET (b), the graph explains the exact nature of FRET and shows why it can be utilised as a 'molecular ruler'. At 50 % FRET efficiency, the  $R_0$  value is calculated and usually expressed in nanometers



Lakowicz 2006). The  $R_0$  distance is defined by the spectral properties of the FRET pair, and represents the distance at which  $E$  is 50 % (Lakowicz 2006):

$$R_0^6 = 8.79 \cdot 10^{-5} [\kappa^2 J(\lambda) n^{-4} Q_D],$$

where  $\kappa^2$  is the orientation factor between the two fluorophores,  $Q_D$  is the donor quantum yield and  $J(\lambda)$  represents the overlap of donor emission and acceptor absorbance spectra. The overlap integral  $J(\lambda)$  is defined as (Lakowicz 2006):

$$J(\lambda) = \int F_D(\lambda) \varepsilon_A(\lambda) \lambda^4 d\lambda,$$

where  $F_D(\lambda)$  is the normalised fluorescence emission and  $\varepsilon_A(\lambda)$  is the molar extinction coefficient of the acceptor absorbance spectrum (Lakowicz 2006).

Distances between 1 and 10 nm can be measured using FRET, making its application in cellular imaging ideal for the visualisation of interactions on the nm length scale (Wu and Brand 1994; Clegg 1995; Patterson et al. 2000; Akrap et al. 2010). The continued development of fluorophores has enabled FRET applications in life sciences, where elucidation of signalling pathways and/or partners is often dependent on the ability to resolve transient interactions of multiple biomolecules.

In order to 'pair' fluorophores for use in measuring FRET, they must fulfil a number of criteria. Firstly, for optimal FRET, the spectral overlap between donor fluorescence and acceptor absorbance must be as large/extensive as possible. Additionally, the donor quantum yield and acceptor extinction coefficient must be as high as possible. Intensity-based FRET furthermore requires a bright acceptor so that the FRET-induced 'sensitised' emission can be easily detected. Lastly, the angular orientation of dipole transition moments of the donor and acceptor fluorophores is an important factor in the efficiency of FRET. This is described by the orientation factor  $\kappa^2$  in the description of  $R_0$ , and its values can range between 0 and 4. A value of 0 corresponds to a perpendicular orientation of donor and acceptor dipole moments, which is not capable of FRET, and 4 corresponds to a collinear orientation which results in maximal FRET efficiency. In a completely averaging regime, where fluorophores are assumed to possess complete rotational freedom, the statistical average over all sampled orientations amounts to a value for  $\kappa^2$  of  $2/3$ . This value is typically used for the calculation of  $R_0$  values in lists of FRET pairs. However, if the FRET pairs are connected to interacting proteins, steric restrictions apply that invalidate the assumption of a  $\kappa^2$  of  $2/3$ . Thus, the value for  $R_0$  might significantly deviate from the expected values that are based on the averaging regime. This

is also the reason why great care should be taken in the estimation of separation distances from FRET efficiencies.

In measuring FRET, these requirements are not always able to be optimised. Maximising spectral overlap introduces bleed-through of donor emission to the acceptor channel and the excitation of the acceptor at donor wavelengths, problems that require extensive correction in sensitised emission FRET (Berney and Danuser 2003). As a large section of the available spectral window is occupied when the emission of two fluorophores is monitored, the use of multiple FRET pairs often difficult (He et al. 2005; Ai et al. 2008).

## FLIM

FRET between donor and acceptor fluorophores quench the donor fluorescence in proportion to the efficiency of FRET as the fluorescence lifetime is proportional to the fluorophores' 'specific brightness', i.e., its quantum yield. This change in lifetime can be observed by fluorescence lifetime imaging microscopy (FLIM) (Bastiaens and Squire 1999; Lakowicz 2006).

As the fluorescence lifetime is an intrinsic property of a particular fluorophore and independent of fluorophore concentration, FLIM is advantageously compared to intensity-based FRET measurements. In contrast to intensity-based FRET measurements, donor lifetime measurements suffice to detect environmental changes, and the measurement puts no demands on the acceptor quantum yield characteristics (Bastiaens and Squire 1999; Chen et al. 2003). It is even possible, and in some cases beneficial, to utilise non-fluorescent acceptors to measure FRET-FLIM (Ganesan et al. 2006). The use of 'dark' acceptors in FLIM measurements allows wider detection range for donor emission. More advanced FRET-FLIM measurements that involve the switching of the absorption properties of the acceptor, such as pcFRET, can be used (Subach et al. 2010; Petchprayoon and Marriott 2010; Don Paul et al. 2013).

FLIM is generally subdivided into time domain (TD) or frequency domain (FD) methods (Chen et al. 2003; van Munster and Gadella 2005). Both approaches follow the effects succeeding an excited fluorophore, but the acquisition and analysis of the data differ. In TD FLIM, fluorophores are excited by a train of very short discrete light pulses. The decay kinetics of the excited state are sampled by measuring the arrival time of the first photon with respect to the excitation pulse. FD FLIM, on the other hand, typically uses a periodically modulated light source, rather than light pulses, to determine the modulation in the emission signal that is generated by the duration of the excited state. This distortion causes changes in the time-integrated signal on a regular charge-coupled device (CCD) camera, from which the fluorescence lifetime can then be estimated. Both modes can be used in

wide-field and scanning microscopes. Most common set-ups for FD FLIM utilise wide-field microscopy whilst TD FLIM is mostly based on laser scanning microscopy. The difference in methodology can be reflected in their biological applications with FD FLIM being faster and therefore applied to living cells, whilst TD FLIM requires longer acquisition times and therefore preferentially used in fixed samples.

### Time domain FLIM techniques

In TD FLIM, very short pulses (femtoseconds to picoseconds) of light are used to sample the fluorescence decay of a fluorophore. Following data acquisition, the shape of the decay function is fitted to an exponential decay model to determine its fluorescence lifetime. The most common implementation is time-correlated single photon counting (TCSPC) where the arrival time of many single emitted photons are recorded with respect to the excitation laser pulse for the different scanned positions in the image.

Current detectors exhibit 'dead times', i.e., a delay time in which the detector cannot record a new photon, that are long with respect to the lifetime, typically in the  $\mu\text{s}$  range. As most fluorophores have fluorescence lifetimes of a few ns, a large number of photons are missed by the detector while it resets. Recording a time-resolved decay curve from a single excitation burst of a fluorophore would require extremely fast detectors with a time resolution in the tens of picoseconds. As no such detector currently exists, TCSPC FLIM uses a periodic excitation scheme extended over multiple excitation events. In this way, a decay curve is reconstructed from single photon events collected over many cycles (Fig. 3a). In order to unambiguously assign the emission photon to the excitation event, the emission probability per event is kept low. As not every excitation pulse generates a photon, the excitation pulse immediately following a detected photon incident is used as a time reference in a 'reverse start-stop' procedure (Fig. 3b).

One major disadvantage of TCSPC FLIM is the long acquisition time. It can take up to 10 min or longer to gather enough photons for a reliable lifetime fitting procedure. In most cases, the count rates of TCSPC FLIM systems are not the limiting factor. Count rates of TCSPC FLIM systems can range up to ten megacounts per second and is limited mainly by the photostability of the dye and the scanning speed of the microscope but not by the counting ability of the detection system (Becker et al. 2004; Katsoulidou et al. 2007; Becker et al. 2009). The optimisation for brightness of fluorophores like mCerulean3 (Markwardt et al. 2011) or mTurquoise2 (Goedhart et al. 2012) is one way to reduce the acquisition times. Additionally, the use of less photon-demanding fitting routines, e.g., Bayesian fitting (Rowley et al. 2011), can be used to reduce the acquisition times.

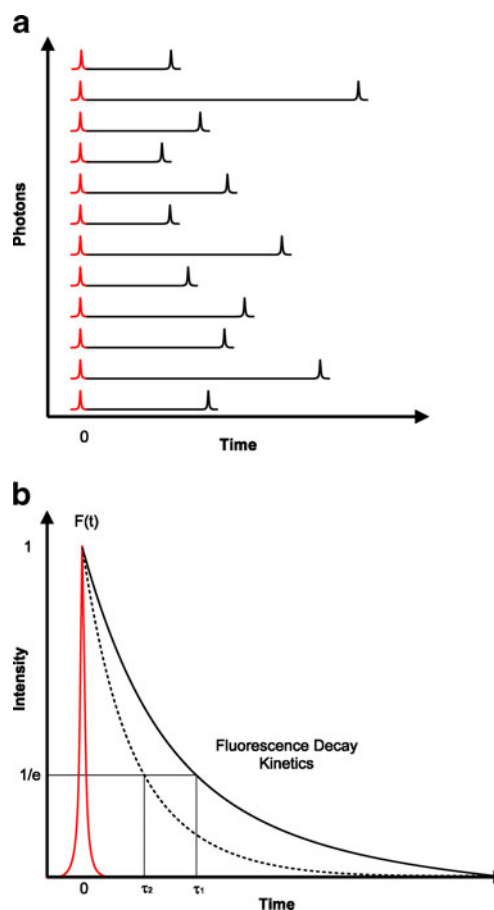


**Fig. 3** An initial short excitation pulse (*red peak*) excites fluorophores in a sample into an excited state. The time between the excitation pulse and detection of the emitted photon is recorded and this process repeated as many times as required to build an accurate decay profile (**a**). Following the recording of numerous arrival times of photons, a fluorescence decay kinetic profile can be calculated (**b**). A decrease  $\tau$  of a donor (*solid line*) indicates an interaction with another chromophore or quencher or is due to changed environmental factors (*dashed line*). The corresponding time at an intensity of  $1/e$  denotes the fluorophores lifetime (*dotted lines*)

While TCSPC FLIM aims to reconstruct the fluorescent decay profile by timing single photon events, an alternative method of sampling decay kinetics after a brief light pulse is to record photons in consecutive time bins. At the core of a time-gated FLIM system is the image intensifier. On arrival of photons at the photocathode, photoelectrons are produced by the photoelectric effect, which are then multiplied thousand-fold in the multichannel plate before generating photons on the anode phosphor screen that are imaged by a CCD camera. The image intensifier can be gated in time with high temporal resolution by application of a gating pulse (Dymoke-Bradshaw 1993). As the intensifier gating is synchronised with the pulsed excitation signal, the camera is opened in the same relative period in successive excitation cycles, gaining time-integrated signals of the decay at arbitrary total exposure times (Fig. 4). The decay is sampled at two or more positions in time. In case of two time gates of equal width and a mono-

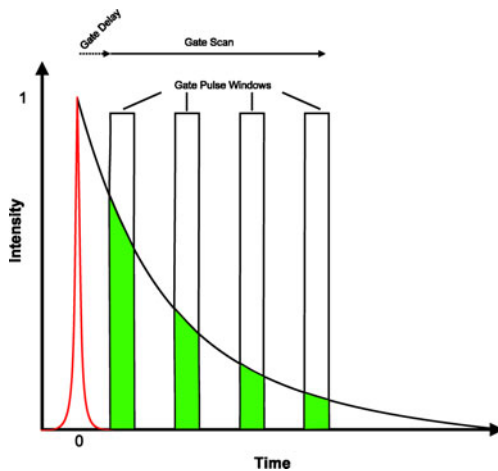


**Fig. 4** A short excitation pulse (*red peak*), excites fluorophores in a sample and following a short delay, a series of gated pulse windows (*white columns*) are 'opened'. Photons emitted from excited fluorophores arriving at the detector within these windows are recorded (*green columns*). By varying the number and 'time' these gates are open, an exponential curve estimating a fluorophores lifetime can be determined

exponential fluorescence decay, the fluorescence lifetime can be easily determined from the ratio of the recorded intensities by the rapid lifetime determination (RLD) formula (Ballew and Demas 1991):

$$\tau = \frac{\Delta\tau}{\ln(I_1/I_0)},$$

where  $I_0$  and  $I_1$  represent the images recorded in the first and second time bin and  $\Delta\tau$  is the gating time. For multi-exponential decay kinetics, the time-gating implementation with two time gates yields an average lifetime, which is sufficient to provide lifetime contrast of biological probes. More than two time gates have been shown to provide quantitative results for biological samples containing multi-exponential decays (Scully et al. 1997; Esposito and Wouters 2004).

Time-gated image intensifiers can be used with scanning microscopes (Wang et al. 1991; Cole et al. 2001; Webb et al. 2002) but more interesting is the combination with wide-field set-ups because the CCD chip based detection system allows the simultaneous acquisition of all spatial information at once, translating in an increase in acquisition speed compared to sampling the image by scanning (Wang et al. 1992; Scully et al. 1996; Dowling et al. 1997). A faster way to record time-gated FLIM on a scanned system is via multi-beam scanning as described by (Straub and Hell 1998).

The image analysis of the RLD method affords significantly shorter calculation time and is surprisingly robust and effective at providing lifetime-based contrasts in biological probes in real time (Ballew and Demas 1989; Esposito et al. 2007). The acquisition times are generally shorter than

techniques based on spatial scanning. As the number of time gates is inversely proportional to photon counting efficiency, the more time gates used to sample the decay function, the fewer photons will be recorded.

The problem of photon efficiency can be eased by recording in only a few time gates in combination with a single-shot detection configuration. Single-shot detection splits an image into two or more images using a beam splitter and each image is designated to a different time bin. In one implementation, one of the two images was projected immediately onto the gated image intensifier while the other image was delayed by taking a detour of several meters before being projected onto the same detector (Agronskaia et al. 2003). For simultaneous, parallel detection, the system is equipped with a four-channel optical splitter working in conjunction with a segmented gated image intensifier. Unlike a conventional image intensifier, the photocathode is subdivided into four quadrants by resistive sectioning, providing four channels, which can be gated at different delay times. The image splitter can therefore relay four sub-images of the sample onto four quadrants of the detector (Elson et al. 2004).

Despite the obvious speed advantage of gated wide-field FLIM setups, it should be noted that the lack of confocal out-of-focus light rejection can cause the mixing of fluorescent signals with different lifetime characteristics, thereby reducing lifetime contrast.

### TD FLIM image analysis

Despite the relative simplicity and speed of the RLD method (Ballew and Demas 1989), it only estimates the average lifetime of all lifetime components weighted by their individual contribution to the mixture. Most FLIM applications in life sciences must deal with multi-exponential decays, derived from mixtures of fluorophores, spectrally similar but possessing different lifetimes. The average fluorescence lifetime can be useful in the case of FRET as it provides contrast between the quenched and unquenched donor. However, due to the fact that the decay curve is strongly under sampled, it is not possible to extract single lifetimes from multi-exponential decay curves. Consequently, determining fractions of donor molecules, which do or do not engage in FRET is not easily possible.

The only technique providing direct access to parameters of multi-exponential decays is TCSPC FLIM. The data from TCSPC measurements usually consists of a large number of photons recorded in a many time channels for each pixel of an image. These photon numbers and corresponding time channels resemble fluorescence decay curves in each pixel of the image. Importantly, at this stage, the data is still a convolution of fluorophore data and the instrument response function (IRF). The IRF is the response of the detection system to only

the excitation pulse and can be measured or calculated from the decay function by Fourier analysis. The deconvolved decay curve can then be fitted to a mathematical model of choice until the best fit is achieved (O'Connor 1984).

### Frequency domain FLIM techniques

FD FLIM employs an excitation light source which is periodically modulated in intensity rather than a train of very short excitation light pulses. The emitted fluorescence is shifted in phase and the amplitude is demodulated relative to the excitation light. The distortion in the temporal emission profile resulting from the time that a fluorophore spends in an excited state before emitting a photon is used to estimate the fluorescence lifetime (Fig. 5). The modulation of the excitation can be a sinusoidal or block wave. Sine wave excitation will result in an emission sine wave of the same frequency, but shifted in phase ( $\phi$ ) and with reduced amplitude. A block wave signal will lose higher-order frequencies as the emission will 'smear out' the sharp edges of the block wave. Provided that a lifetime is long enough, the block wave will result in a sine wave at the fundamental modulation frequency. These effects are described in (Lakowicz 2006):

$$\tau_{\phi} = \frac{\tan(\phi)}{\omega}$$

$$\tau_M = \sqrt{\frac{1-M}{M\omega}}$$

where  $\tau_{\phi}$  is the phase lifetime,  $\phi$  is the phase shift at every modulation frequency  $\omega$ ,  $\tau_M$  is the modulation lifetime and  $M$  is the modulation.

The emission function is therefore 'dampened' according to the fluorescence lifetime of the fluorophore. An analogue from elementary school physics helps us to intuitively understand the connection between lifetime, phase delay and the

reduction in amplitude. Imagine a movable arm (modulated excitation) connected to a spring and a weight. Oscillation of the arm moves the weight and compared to the movement of the arm, movement of the weight is delayed in time and its amplitude is reduced. The parameter that defines delay and demodulation is the spring constant. In our model, it is equivalent to the fluorescence lifetime. A small spring constant/lifetime will result in a small phase delay while a large spring constant/lifetime will cause a large phase delay. The amplitude will be larger for small lifetimes and smaller for large lifetimes.

As biological fluorophores usually possess fluorescence lifetimes in the nanosecond range, the excitation intensity is modulated at tens of Megahertz. If the modulation frequency is too low, the fluorescence will decay before the excitation cycle is completed. If the excitation frequency is too high, excited fluorophores will still be emitting whilst the excitation cycle starts again leading to saturation and an averaging-out of the modulation. Different lifetime components in a sample therefore require multiple frequencies (Colyer et al. 2008). The lifetime of a fluorophore can be determined directly via its phase delay or modulation ratio at different modulation frequencies. For single exponential decays, if the decay kinetics are best fit to a single exponential decay function, the lifetime phase shift and modulation change will be the same at all frequencies. If the decay is multi-exponential, then the lifetime phase shift will be smaller than the lifetime modulation change and their values will depend on the modulation frequency. Therefore, FD FLIM provides immediate information on lifetime heterogeneity.

The high acquisition speeds of FD FLIM make it an ideal technique for fluorescence lifetime measurements of living cells. One of the reasons why, nevertheless, TD equipment is more widely implemented in laboratories and imaging facilities is the relative complexity of FD equipment. Particularly, the image intensifier is an expensive and vulnerable component that, additionally, degrades the image quality.

For this reason, complete camera-based systems for FLIM will likely replace the conventional image intensifier-based implementation. We have implemented one such all-solid-state camera solution for FD FLIM. Based on the detector

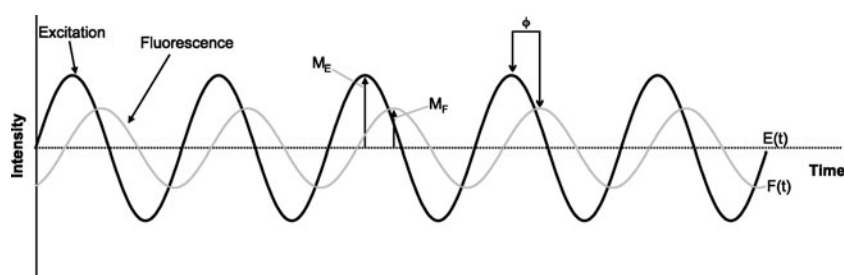


**Fig. 5** Excitation light is modulated at a known frequency, usually in a sinusoidal manner (black line). Upon excitation of a fluorophore, light emitted as fluorescence (grey line) is altered in its amplitude and

frequency. The change in magnitude ( $M$ ) and phase ( $\phi$ ) can be used to determine the fluorescence lifetime of a fluorophore



design of a real-time time-of-flight 3D ranging camera (Lange et al. 1999), the FLIM camera demodulates the periodic emission signal in the pixel substrate of the detector chip directly (Oggier et al. 2004; Esposito et al. 2005). To this end, photoelectrons generated in a central photo-sensitive area of the pixel are sorted between two connected collection bins that are charged at opposite phase and that are cycled in synchrony with the modulation signal driving the laser source throughout the acquisition of the image. At the end of the acquisition period, both bins are read out and their relative content is representative of the average fluorescence lifetime of the sample.

This imaging mode is the FD equivalent of the RLD in the TD. By taking multiple images at different phase settings, the camera can be run as a conventional image intensifier-based FD FLIM for higher lifetime resolution. The major advantage of the RLD modus, though, besides its high speed (up to 50 Hz full-frame FLIM), is the fact that both sub-images, i.e., the content of both collection bins per pixel, are acquired during the same acquisition. This parallel acquisition is not given in any other implementation of FLIM and renders the measurement insensitive to sample movement and bleaching artefacts.

The photoelectron sorting process can best be understood as the product of the probability of photon arrival (due to the periodic intensity modulation of the laser) and the sorting probability of the pixels (due to the modulation of the bin charge). The peak of the sine-wave modulated laser intensity will produce the highest photoelectron production in the pixel. For a zero lifetime emission signal, the peak intensity will coincide with the largest charge difference between the bins. In this state, the photoelectrons are maximally attracted to the positively charged, and maximally repulsed by the negatively charged bin, filling only one bin. With increasing lifetime, photoelectrons are generated with a delay relative to the excitation-synchronised sorting cycle and an increasing amount of photoelectrons escape collection in this bin and end up in the other. This detection principle is repeated in every pixel of the detector, yielding FLIM images at very high temporal and spatial resolution (Fig. 6).

### FD FLIM image analysis

FD FLIM techniques are often the best choice for FRET measurements in living cells as image acquisition is rapid

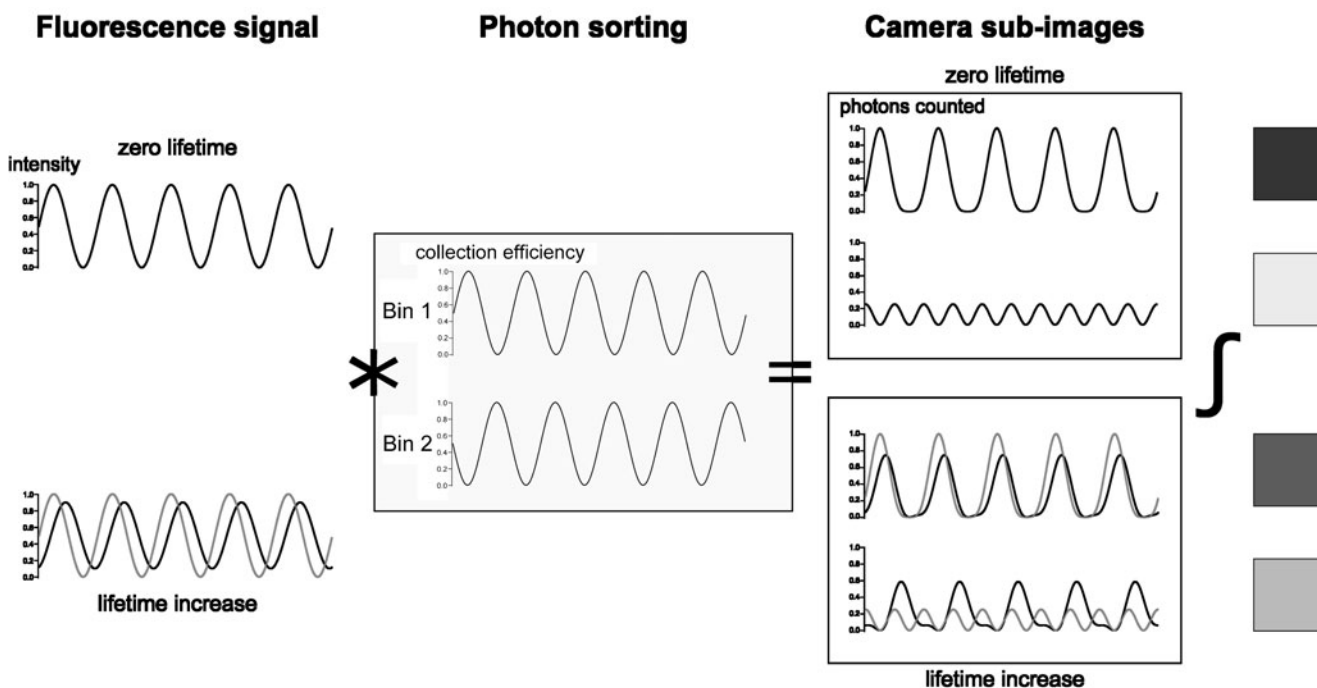


**Fig. 6** The time-modulated emission signals (*left*) are shifted in phase and demodulated with respect to the excitation signal. For a lifetime of zero, e.g., reflected light, the emission signal is identical to the excitation signal (*upper image*), with increasing lifetime of the fluorophore, the emission signal will experience an increasing phase shift and demodulation (*lower image*, zero lifetime situation shown in grey). The camera (*middle block*) acts as a mixer for the emission signal and the excitation signal: the sorting efficiency of both collection bins are shown. The sorting efficiency of Bin 1 follows the excitation signal and that of bin 2 is modulated in opposite phase. This way, the sorting probability cycles

between both bins in time in synchrony with the excitation signal. The results of the mixing process, i.e., image formation in the camera from both bins, are shown on the *right*. For a zero lifetime signal (*upper*), the photoelectrons are sorted almost exclusively in Bin 1. For increasing lifetimes (*lower*; zero lifetime reference shown in grey), less photoelectrons are sorted to Bin 1 and more to Bin 2. The integrated photoelectron content of both Bins are read out as images. From the intensity distribution between both simultaneously acquired images, the lifetime can be estimated

and can reach video rates (Redford and Clegg 2005). Measurements are commonly analysed using a polar plot or phasor plot. This offers a simple, graphical and rapid algorithm for interpreting the phase and modulation data of a single frequency measurement, which is of great assistance in the interpretation of phase and modulation information and the actual lifetime distribution. The measured variables are transferred to a coordinate system with changed coordinates:  $x=M(\omega)\times\cos\Phi(\omega)$  and  $y=M(\omega)\times\sin\Phi(\omega)$ . A vector of the magnitude  $M(\omega)$  is projected onto a polar angular coordinate  $\Phi(\omega)$  giving rise to a two-dimensional histogram (phasor) that describes the trajectory of any single lifetime distribution.

The simple mapping of data points in a phasor plot allow the immediate quantification of mixtures and FRET efficiencies. The phasor plot can also be utilised in a reciprocal manner, where each occupied point is used as a spectroscopic marker for a fluorophore that can be mapped to a pixel of an image to offer a means of identifying molecules by the position in the phasor plot (Redford and Clegg 2005; Digman et al. 2008). This form of image-guided look-up analysis and data segmentation is very powerful for the interpretation of cellular responses that are, necessarily of a complex spectroscopic nature.

### Endogenous fluorophores in cell and tissue

Autofluorescence arising from biological tissue and cells is often considered background noise that contaminates the 'true' signal and is therefore generally avoided when imaging. Autofluorescence, however, is a complex mixture of various fluorophores whose emission span the entire spectrum. It can be utilised as an endogenous label of specific metabolites or structures whose alterations can be used as a diagnostic tool.

The major sources of autofluorescence in mammalian tissue are FAD and NADH, both of which play a pivotal role in cellular energy metabolism as major electron acceptors. The relative amount of their oxidised or reduced forms can be broadly assumed to be indicative of the energy status of a cell. The conjugated ring structures of FAD and NADH give rise to fluorescence of the oxidised or reduced form, respectively. NADH exhibits a fluorescence emission maximum at 460 nm, FAD emits at 525 nm and the ratio between signals measured at these wavelengths is indicative of the redox state of cells and tissues (Chance 1976; Chance et al. 1979). FLIM experiments have also shown that two distinct lifetimes can be observed for NADH and FAD, depending on whether they are bound to protein (Nakashima et al. 1980; Lakowicz et al. 1992). As the ratio between protein bound:free NADH or FAD is indicative of the metabolic state of the cell, fluorescence lifetime analysis of these compounds can be used as a diagnostic tool for changes in cellular metabolism in cancer (Drezerk et al. 2001; Ramanujam et al. 2001; Zhang et al.

2004; Kantelhardt et al. 2007; Skala et al. 2007). In clinical applications the non-invasive nature of FLIM has been used to discriminate between healthy and cancer tissue *in vivo* by analysing the metabolic state of those tissues. In order to expand the use of FLIM towards intra-operative application, FLIM-based endoscopes have been developed to enable mapping of cancerous tissue during surgery (Elson et al. 2007; Sun et al. 2009; Fatakdawala et al. 2013). Fatakdawala and colleagues combine FLIM together with ultrasound backscattering microscopy and photoacoustic imaging within one endoscope probe head in order to determine the exact three-dimensional spreading of oral cancer to assist the surgeon (Fatakdawala et al. 2013).

Apart from cancer diagnostics, FLIM has also been applied in the field of ophthalmology, where it has been used to map age- or disease-related changes in the fundus of the human eye (Feeney-Burns et al. 1980; Eldred and Katz 1988; Delori et al. 1995; Ishibashi et al. 1998). FLIM has been used to detect the aging related pigment lipofuscin that emits in the yellow to red spectrum (von Rückmann et al. 1995; von Rückmann et al. 2002; Einbock et al. 2004; Bindewald 2005; Schweitzer et al. 2007). Furthermore, advanced glycation end products, collagen as well as elastin are of special interest in the diagnosis of age-related macular degeneration, diabetic retinopathy or glaucoma. Early detection of sclerotic and degenerative processes enhances the ability for successful medical intervention, making the eye a window to the rest of the body (Schweitzer et al. 2007).

The combination of FLIM and second harmonics generation (Fine and Hansen 1971; Freund et al. 1986; Freund and Deutsch 1986) extends this method and provides valuable additional diagnostic information (König and Riemann 2003; Dimitrow et al. 2009; Sanchez et al. 2010; König et al. 2011).

### Concluding remarks

There should be little doubt of the importance that FLIM has played in the life sciences and in biological imaging in the last decade. FLIM, as fluorescence microscopy itself, would not have gained its current popularity and utility without the generation and continuous improvement of available fluorophores. Ranging from some of the smallest molecules endogenously available in a cell to synthetic conjugatable dyes and autofluorescent proteins purified from a marine jellyfish, fluorophores have enabled us to visualise a multitude of events within a cell. There have been significant advances in technical instrumentation and analytical approaches for the quantification of fluorescent signals. The use of custom-tailored fluorophores and assays in techniques like FRET-FLIM have allowed the detection of interactions between molecules at the (sub)nanometer level. The tremendous

increase in publications that use these techniques are testament to the increase in our understanding of cellular molecular events that they have permitted. In amongst all of these developments in imaging, fluorescence lifetime-based techniques, have only over the last 10–15 years, started to be utilised to their full potential.

**Acknowledgements** This work was supported by the Cluster of Excellence and DFG Research Center for Nanoscale Microscopy and Molecular Physiology of the Brain.

**Conflict of interest** None

## References

- Abad MFC, Di Benedetto G, Magalhães PJ, Filippin L, Pozzan T (2004) Mitochondrial pH monitored by a new engineered green fluorescent protein mutant. *J Biol Chem* 279:11521–11529
- Agronskaia AV, Tertoolen L, Gerritsen HC (2003) High frame rate fluorescence lifetime imaging. *J Phys Appl Phys* 36:1655–1662
- Ai H, Hazelwood KL, Davidson MW, Campbell RE (2008) Fluorescent protein FRET pairs for ratiometric imaging of dual biosensors. *Nat Methods* 5:401–403
- Åkerman ME, Chan WC, Laakkonen P, Bhatia SN, Ruoslahti E (2002) Nanocrystal targeting in vivo. *Proc Natl Acad Sci* 99:12617–12621
- Akrap N, Seidel T, Barisas BG (2010) Förster distances for fluorescence resonant energy transfer between mCherry and other visible fluorescent proteins. *Anal Biochem* 402:105–106
- Ballew RM, Demas JN (1991) Error analysis of the rapid lifetime determination method for single exponential decays with a non-zero baseline. *Anal Chim Acta* 245:121–127
- Ballew RM, Demas JN (1989) An error analysis of the rapid lifetime determination method for the evaluation of single exponential decays. *Anal Chem* 61:30–33
- Bastiaens PI, Squire A (1999) Fluorescence lifetime imaging microscopy: spatial resolution of biochemical processes in the cell. *Trends Cell Biol* 9:48–52
- Becker W (2012) Fluorescence lifetime imaging — techniques and applications. *J Microsc* 247:119–136
- Becker W, Bergmann A, Biscotti G, Koenig K, Riemann I, Kelbouskas L, Biskup C (2004) High-speed FLIM data acquisition by time-correlated single-photon counting. *Biomed. Opt.* 27–35
- Becker W, Su B, Bergmann A (2009) Fast-acquisition multispectral FLIM by parallel TCSPC. *SPIE Proc* 7183:718305–718305, 5
- Berney C, Danuser G (2003) FRET or no FRET: a quantitative comparison. *Biophys J* 84:3992–4010
- Bindewald A (2005) Lower limits of fluorescein and indocyanine green dye for digital cSLO fluorescence angiography. *Br J Ophthalmol* 89:1609–1615
- Bruchez MP (2011) Quantum dots find their stride in single molecule tracking. *Curr Opin Chem Biol* 15:775–780
- Bulina ME, Chudakov DM, Britanova OV, Yanushevich YG, Staroverov DB, Chepurnykh TV, Merzlyak EM, Shkrob MA, Lukyanov S, Lukyanov KA (2005) A genetically encoded photosensitizer. *Nat Biotechnol* 24:95–99
- Bunt G, Wouters FS (2004) Visualization of molecular activities inside living cells with fluorescent labels. *Int Rev Cytol* 237:205–277
- Chalfie M, Tu Y, Euskirchen G, Ward WW, Prasher DC (1994) Green fluorescent protein as a marker for gene expression. *Science* 263:802–805
- Chan WC, Nie S (1998) Quantum dot bioconjugates for ultrasensitive nonisotopic detection. *Science* 281:2016–2018
- Chance B (1976) Pyridine nucleotide as an indicator of the oxygen requirements for energy-linked functions of mitochondria. *Circ Res* 38:131–138
- Chance B, Schoener B, Oshino R, Itshak F, Nakase Y (1979) Oxidation-reduction ratio studies of mitochondria in freeze-trapped samples. NADH and flavoprotein fluorescence signals. *J Biol Chem* 254:4764–4771
- Chen F, Gerion D (2004) Fluorescent CdSe/ZnS nanocrystal-peptide conjugates for long-term, nontoxic imaging and nuclear targeting in living cells. *Nano Lett* 4:1827–1832
- Chen Y, Mills JD, Periasamy A (2003) Protein localization in living cells and tissues using FRET and FLIM. *Differentiation* 71:528–541
- Clegg RM (1995) Fluorescence resonance energy transfer. *Curr Opin Biotechnol* 6:103–110
- Cole MJ, Siegel J, Webb SED, Jones R, Dowling K, Dayel MJ, Parsons-Karavassilis D, French PMW, Lever MJ, Sucharov LOD (2001) Time-domain whole-field fluorescence lifetime imaging with optical sectioning. *J Microsc* 203:246–257
- Colyer RA, Lee C, Gratton E (2008) A novel fluorescence lifetime imaging system that optimizes photon efficiency. *Microsc Res Tech* 71:201–213
- Cubitt AB, Heim R, Adams SR, Boyd AE, Gross LA, Tsien RY (1995) Understanding, improving and using green fluorescent proteins. *Trends Biochem Sci* 20:448–455
- Cui B, Wu C, Chen L, Ramirez A, Bearer EL, Li W-P, Mobley WC, Chu S (2007) One at a time, live tracking of NGF axonal transport using quantum dots. *Proc Natl Acad Sci* 104:13666–13671
- Delori FC, Staurengi G, Arend O, Dorey CK, Goger DG, Weiter JJ (1995) In vivo measurement of lipofuscin in Stargardt's disease—fundus flavimaculatus. *Invest Ophthalmol Vis Sci* 36:2327–2331
- Digman MA, Caiolfa VR, Zamai M, Gratton E (2008) The phasor approach to fluorescence lifetime imaging analysis. *Biophys J* 94:L14–L16
- Dimitrow E, Riemann I, Ehlers A, Koehler MJ, Norgauer J, Elsner P, König K, Kaatz M (2009) Spectral fluorescence lifetime detection and selective melanin imaging by multiphoton laser tomography for melanoma diagnosis. *Exp Dermatol* 18:509–515
- Don Paul C, Kiss C, Traore DAK, Gong L, Wilce MCJ, Devenish RJ, Bradbury A, Prescott M (2013) Phanta: a non-fluorescent photochromic acceptor for pcFRET. *PLoS ONE* 8:e75835
- Don Paul C, Traore DAK, Byres E, Rossjohn J, Devenish RJ, Kiss C, Bradbury A, Wilce MCJ, Prescott M (2011) Expression, purification, crystallization and preliminary X-ray analysis of eCGP123, an extremely stable monomeric green fluorescent protein with reversible photoswitching properties. *Acta Crystallograph Sect F Struct Biol Cryst Commun* 67:1266–1268
- Dowling K, Hyde SCW, Dainty JC, French PMW, Hares JD (1997) 2-D fluorescence lifetime imaging using a time-gated image intensifier. *Opt Commun* 135:27–31
- Drezek R, Brookner C, Pavlova I, Boiko I, Malpica A, Lotan R, Follen M, Richards-Kortum R (2001) Autofluorescence microscopy of fresh cervical-tissue sections reveals alterations in tissue biochemistry with dysplasia. *Photochem Photobiol* 73:636–641
- Dubertret B, Skourides P, Norris DJ, Noireaux V, Brivanlou AH, Libchaber A (2002) In vivo imaging of quantum dots encapsulated in phospholipid micelles. *Science* 298:1759–1762
- Dymoke-Bradshaw AKL (1993) Impact of high-voltage pulse technology on high-speed photography. *Proc SPIE* 1757:2–6
- Einbock W, Moessner A, Schnurbusch UEK, Holz FG, Wolf S, for the FAM Study Group (2004) Changes in fundus autofluorescence in patients with age-related maculopathy. Correlation to visual function: a prospective study. *Graefes Arch Clin Exp Ophthalmol* 243:300–305

- Eldred GE, Katz ML (1988) Fluorophores of the human retinal pigment epithelium: separation and spectral characterization. *Exp Eye Res* 47:71–86
- Elson D, Requejo-Isidro J, Munro I, Reavell F, Siegel J, Suhling K, Tadrous P, Benninger R, Lanigan P, McGinty J (2004) Time-domain fluorescence lifetime imaging applied to biological tissue. *Photochem Photobiol Sci* 3:795–801
- Elson DS, Jo JA, Marcu L (2007) Miniaturized side-viewing imaging probe for fluorescence lifetime imaging (FLIM): validation with fluorescence dyes, tissue structural proteins and tissue specimens. *New J Phys* 9:127–127
- Esposito A, Dohm CP, Bähr M, Wouters FS (2007) Unsupervised fluorescence lifetime imaging microscopy for high content and high throughput screening. *Mol Amp Cell Proteomics* 6:1446–1454
- Esposito A, Oggier T, Gerritsen H, Lustenberger F, Wouters F (2005) All-solid-state lock-in imaging for wide-field fluorescence lifetime sensing. *Opt Express* 13:9812–9821
- Esposito A, Wouters FS (2004) Fluorescence lifetime imaging microscopy. *Curr Protoc Cell Biol Editor Board Juan Bonifacino AI Chapter 4:Unit 4.14*
- Faltin B, Zengerle R, von Stetten F (2013) Current methods for fluorescence-based universal sequence-dependent detection of nucleic acids in homogenous assays and clinical applications. *Clin Chem* 59:1567–1582
- Fatakawala H, Poti S, Zhou F, Sun Y, Bec J, Liu J, Yankelevich DR, Tinling SP, Gandour-Edwards RF, Farwell DG, Marcu L (2013) Multimodal in vivo imaging of oral cancer using fluorescence lifetime, photoacoustic and ultrasound techniques. *Biomed Opt Express* 4:1724–1741
- Feeney-Burns L, Berman ER, Rothman H (1980) Lipofuscin of human retinal pigment epithelium. *Am J Ophthalmol* 90:783–791
- Fine S, Hansen WP (1971) Optical second harmonic generation in biological systems. *Appl Opt* 10:2350–2353
- Förster T (1948) Zwischenmolekulare Energiewanderung und Fluoreszenz. *Ann Phys* 437:55–75
- Freund I, Deutsch M (1986) Second-harmonic microscopy of biological tissue. *Opt Lett* 11:94
- Freund I, Deutsch M, Sprecher A (1986) Connective tissue polarity. Optical second-harmonic microscopy, crossed-beam summation, and small-angle scattering in rat-tail tendon. *Biophys J* 50:693–712
- Ganesan S, Ameer-Beg SM, Ng TT, Vojnovic B, Wouters FS (2006) A dark yellow fluorescent protein (YFP)-based Resonance Energy-Accepting Chromoprotein (REACH) for Förster resonance energy transfer with GFP. *Proc Natl Acad Sci U S A* 103:4089–4094
- Gill R, Le Ru EC (2011) Fluorescence enhancement at hot-spots: the case of Ag nanoparticle aggregates. *Phys Chem Chem Phys* 13:16366
- Goedhart J, von Stetten D, Noircleerc-Savoye M, Lelimosin M, Joosen L, Hink MA, van Weeren L, Gadella TWJ Jr, Royant A (2012) Structure-guided evolution of cyan fluorescent proteins towards a quantum yield of 93 %. *Nat Commun* 3:751
- Griesbeck O, Baird GS, Campbell RE, Zacharias DA, Tsien RY (2001) Reducing the environmental sensitivity of yellow fluorescent protein. Mechanism and applications. *J Biol Chem* 276:29188–29194
- Gussin HA, Tomlinson ID, Little DM, Warnement MR, Qian H, Rosenthal SJ, Pepperberg DR (2006) Binding of muscimol-conjugated quantum dots to GABA C receptors. *J Am Chem Soc* 128:15701–15713
- He L, Wu X, Simone J, Hewgill D, Lipsky PE (2005) Determination of tumor necrosis factor receptor-associated factor trimerization in living cells by CFP->YFP->mRFP FRET detected by flow cytometry. *Nucleic Acids Res* 33:e61–e61
- Ishibashi T, Murata T, Hangai M, Nagai R, Horiuchi S, Lopez PF, Hinton DR, Ryan SJ (1998) Advanced glycation end products in age-related macular degeneration. *Arch Ophthalmol* 116:1629–1632
- Kantelhardt SR, Leppert J, Krajewski J, Petkus N, Reusche E, Tronnier VM, Hüttmann G, Giese A (2007) Imaging of brain and brain tumor specimens by time-resolved multiphoton excitation microscopy ex vivo. *Neuro-Oncol* 9:103–112
- Katsoulidou V, Bergmann A, Becker W (2007) How fast can TCSPC FLIM be made? *Proc SPIE* 6771:67710B-1–67710B-7
- Kikuchi A, Fukumura E, Karasawa S, Mizuno H, Miyawaki A, Shiro Y (2008) Structural characterization of a thiazoline-containing chromophore in an orange fluorescent protein, monomeric Kusabira orange. *Biochem* 47:11573–11580
- König K, Riemann I (2003) High-resolution multiphoton tomography of human skin with subcellular spatial resolution and picosecond time resolution. *J Biomed Opt* 8:432
- König K, Uchugonova A, Gorjup E (2011) Multiphoton fluorescence lifetime imaging of 3D-stem cell spheroids during differentiation. *Microsc Res Tech* 74:9–17
- Lakowicz JR (2006) Principles of fluorescence spectroscopy. Springer, New York
- Lakowicz JR, Szmacinski H, Nowaczyk K, Johnson ML (1992) Fluorescence lifetime imaging of free and protein-bound NADH. *Proc Natl Acad Sci* 89:1271–1275
- Lange R, Seitz P, Biber A, Schwarte R (1999) Time-of-flight range imaging with a custom solid state image sensor. *Proc SPIE* 1823:180–191
- Llópis J, McCaffery JM, Miyawaki A, Farquhar MG, Tsien RY (1998) Measurement of cytosolic, mitochondrial, and Golgi pH in single living cells with green fluorescent proteins. *Proc Natl Acad Sci* 95:6803–6808
- Mandal G, Darragh M, Wang YA, Heyes CD (2013) Cadmium-free quantum dots as time-gated bioimaging probes in highly-autofluorescent human breast cancer cells. *Chem Commun* 49:624
- Markwardt ML, Kremers G-J, Kraft CA, Ray K, Cranfill PJC, Wilson KA, Day RN, Wachter RM, Davidson MW, Rizzo MA (2011) An improved cerulean fluorescent protein with enhanced brightness and reduced reversible photoswitching. *PLoS One* 6:e17896
- Matz MV, Fradkov AF, Labas YA, Savitsky AP, Zaraisky AG, Markelov ML, Lukyanov SA (1999) Fluorescent proteins from nonbioluminescent Anthozoa species. *Nat Biotechnol* 17:969–973
- McNamara G, Boswell CA (2008) A thousand proteins of light: 15 years of advances in fluorescent proteins. In: Mendez-Vilas A, Diaz J (eds) Modern research and educational topics in microscopy. Formatex, Badajoz, p 287
- Miesenböck G, De Angelis DA, Rothman JE (1998) Visualizing secretion and synaptic transmission with pH-sensitive green fluorescent proteins. *Nature* 394:192–195
- Mitchell GP, Mirkin CA, Letsinger RL (1999) Programmed assembly of DNA functionalized quantum dots. *J Am Chem Soc* 121:8122–8123
- Mitra RD, Silva CM, Youvan DC (1996) Fluorescence resonance energy transfer between blue-emitting and red-shifted excitation derivatives of the green fluorescent protein. *Gene* 173:13–17
- Miyawaki A, Llópis J, Heim R, McCaffery JM, Adams JA, Ikura M, Tsien RY (1997) Fluorescent indicators for Ca<sup>2+</sup> based on green fluorescent proteins and calmodulin. *Nature* 388:882–887
- Nakashima N, Yoshihara K, Tanaka F, Yagi K (1980) Picosecond fluorescence lifetime of the coenzyme of D-amino acid oxidase. *J Biol Chem* 255:5261–5263
- Nann T (2005) Phase-transfer of CdSe@ZnS quantum dots using amphiphilic hyperbranched polyethylenimine. *Chem Commun* 2005:1735–1736
- O'Connor DV (1984) Time-correlated single photon counting. Academic Press, London
- Oggier T, Lehmann M, Kaufmann R, Schweizer M, Richter M, Metzler P, Lang G, Lustenberger F, Blanc N (2004) An all-solid-state optical range camera for 3D real-time imaging with sub-centimeter depth resolution (SwissRanger). *Proc SPIE* 5249:534–545
- Parak WJ, Gerion D, Zanchet D, Woerz AS, Pellegrino T, Micheel C, Williams SC, Seitz M, Bruehl RE, Bryant Z, Bustamante C, Bertozzi CR, Alivisatos AP (2002) Conjugation of DNA to silanized



- colloidal semiconductor nanocrystalline quantum dots. *Chem Mater* 14:2113–2119
- Parak WJ, Pellegrino T, Plank C (2005) Labelling of cells with quantum dots. *Nanotechnology* 16:R9–R25
- Patterson GH, Knobel SM, Sharif WD, Kain SR, Piston DW (1997) Use of the green fluorescent protein and its mutants in quantitative fluorescence microscopy. *Biophys J* 73:2782–2790
- Patterson GH, Piston DW, Barisac BG (2000) Förster distances between green fluorescent protein pairs. *Anal Biochem* 284:438–440
- Pédélecq J-D, Cabantous S, Tran T, Terwilliger TC, Waldo GS (2005) Engineering and characterization of a superfolder green fluorescent protein. *Nat Biotechnol* 24:79–88
- Pellegrino T, Parak WJ, Boudreau R, Gerion D, Alivisatos AP, Larabell CA (2003) Quantum dot-based cell motility assay. *Differentiation* 71:542–548
- Petchprayoon C, Marriott G (2010) Synthesis and spectroscopic characterization of red-shifted spironaphthoxazine based optical switch probes. *Tetrahedron Lett* 51:6753–6755
- Pettikiriachchi A, Gong L, Perugini MA, Devenish RJ, Prescott M (2012) Ultramarine, a chromoprotein acceptor for Förster resonance energy transfer. *PLoS ONE* 7:e41028
- Pons T, Medintz IL, Sapsford KE, Higashiya S, Grimes AF, English DS, Mattoussi H (2007) On the quenching of semiconductor quantum dot photoluminescence by proximal gold nanoparticles. *Nano Lett* 7:3157–3164
- Pons T, Pic E, Lequeux N, Cassette E, Bezdetnaya L, Guillemin F, Marchal F, Dubertret B (2010) Cadmium-free CuInS<sub>2</sub>/ZnS quantum dots for sentinel lymph node imaging with reduced toxicity. *ACS Nano* 4:2531–2538
- Ramanujam N, Richards-Kortum R, Thomsen S, Mahadevan-Jansen A, Follen M, Chance B (2001) Low temperature fluorescence imaging of freeze-trapped human cervical tissues. *Opt Express* 8:335–343
- Redford GI, Clegg RM (2005) Polar plot representation for frequency-domain analysis of fluorescence lifetimes. *J Fluoresc* 15:805–815
- Resch-Genger U, Grabolle M, Cavaliere-Jaricot S, Nitschke R, Nann T (2008) Quantum dots versus organic dyes as fluorescent labels. *Nat Methods* 5:763–775
- Rowley MI, Barber PR, Coolen ACC, Vojnovic B (2011) Bayesian analysis of fluorescence lifetime imaging data. pp 790325–790325–12
- Sanchez WY, Prow TW, Sanchez WH, Grice JE, Roberts MS (2010) Analysis of the metabolic deterioration of ex vivo skin from ischemic necrosis through the imaging of intracellular NAD(P)H by multiphoton tomography and fluorescence lifetime imaging microscopy. *J Biomed Opt* 15:046008
- Schweitzer D, Schenke S, Hammer M, Schweitzer F, Jentsch S, Birkner E, Becker W, Bergmann A (2007) Towards metabolic mapping of the human retina. *Microsc Res Tech* 70:410–419
- Scully AD, MacRobert AJ, Botchway S, O'Neill P, Parker AW, Ostler RB, Phillips D (1996) Development of a laser-based fluorescence microscope with subnanosecond time resolution. *J Fluoresc* 6:119–125
- Scully AD, Ostler RB, Phillips D, O'Neill P, Townsend KMS, Parker AW, MacRobert AJ (1997) Application of fluorescence lifetime imaging microscopy to the investigation of intracellular PDT mechanisms. *Bioimaging* 5:9–18
- Shaner NC, Steinbach PA, Tsien RY (2005) A guide to choosing fluorescent proteins. *Nat Methods* 2:905–909
- Shimomura O, Johnson FH, Saiga Y (1962) Extraction, purification and properties of aequorin, a bioluminescent protein from the luminous hydromedusa, *Aequorea*. *J Cell Comp Physiol* 59:223–239
- Skala MC, Ricking KM, Gendron-Fitzpatrick A, Eickhoff J, Eliceiri KW, White JG, Ramanujam N (2007) In vivo multiphoton microscopy of NADH and FAD redox states, fluorescence lifetimes, and cellular morphology in precancerous epithelia. *Proc Natl Acad Sci* 104:19494–19499
- Straub M, Hell SW (1998) Fluorescence lifetime three-dimensional microscopy with picosecond precision using a multifocal multiphoton microscope. *Appl Phys Lett* 73:1769
- Subach FV, Zhang L, Gadella TWJ, Gurskaya NG, Lukyanov KA, Verkhusha VV (2010) Red fluorescent protein with reversibly photoswitchable absorbance for photochromic FRET. *Chem Biol* 17:745–755
- Sun Y, Phipps J, Elson DS, Stoy H, Tinling S, Meier J, Poirier B, Chuang FS, Farwell DG, Marcu L (2009) Fluorescence lifetime imaging microscopy: in vivo application to diagnosis of oral carcinoma. *Opt Lett* 34:2081–2083
- Terai T, Nagano T (2013) Small-molecule fluorophores and fluorescent probes for bioimaging. *Pflüg Arch - Eur J Physiol* 465:347–359
- Tsien RY (1998) The green fluorescent protein. *Annu Rev Biochem* 67:509–544
- van Munster EB, Gadella TWJ (2005) Fluorescence lifetime imaging microscopy (FLIM). In: Rietdorf J (ed) *Microscopy Techniques*. Springer, Berlin, pp 143–175
- Vegh RB, Solntsev KM, Kuimova MK, Cho S, Liang Y, Loo BLW, Tolbert LM, Bommarius AS (2011) Reactive oxygen species in photochemistry of the red fluorescent protein “Killer Red”. *Chem Commun* 47:4887
- von Rückmann A, Fitzke FW, Bird AC (1995) Distribution of fundus autofluorescence with a scanning laser ophthalmoscope. *Br J Ophthalmol* 79:407–412
- von Rückmann A, Fitzke FW, Fan J, Halfyard A, Bird AC (2002) Abnormalities of fundus autofluorescence in central serous retinopathy. *Am J Ophthalmol* 133:780–786
- Waggoner A (2006) Fluorescent labels for proteomics and genomics. *Curr Opin Chem Biol* 10:62–66
- Walling MA, Novak JA, Shepard JRE (2009) Quantum dots for live cell and in vivo imaging. *Int J Mol Sci* 10:441–491
- Wang Q, Xu Y, Zhao X, Chang Y, Liu Y, Jiang L, Sharma J, Seo D-K, Yan H (2007) A facile one-step in situ functionalization of quantum dots with preserved photoluminescence for bioconjugation. *J Am Chem Soc* 129:6380–6381
- Wang XF, Periasamy A, Herman B, Coleman DM (1992) Fluorescence lifetime imaging microscopy (FLIM): instrumentation and applications. *Crit Rev Anal Chem* 23:369–395
- Wang XF, Uchida T, Coleman DM, Minami S (1991) A two-dimensional fluorescence lifetime imaging system using a gated image intensifier. *Appl Spectrosc* 45:360–366
- Webb SED, Gu Y, Lévêque-Fort S, Siegel J, Cole MJ, Dowling K, Jones R, French PMW, Neil MAA, Juškaitis R, Sucharov LOD, Wilson T, Lever MJ (2002) A wide-field time-domain fluorescence lifetime imaging microscope with optical sectioning. *Rev Sci Instrum* 73:1898
- Wu P, Brand L (1994) Resonance energy transfer: methods and applications. *Anal Biochem* 218:1–13
- Xing Y, Chaudry Q, Shen C, Kong KY, Zhau HE, Chung LW, Petros JA, O'Regan RM, Yezhelyev MV, Simons JW, Wang MD, Nie S (2007) Bioconjugated quantum dots for multiplexed and quantitative immunohistochemistry. *Nat Protoc* 2:1152–1165
- Zhang W, Zhou Y, Becker DF (2004) Regulation of PutA–membrane associations by flavin adenine dinucleotide reduction. *Biochem* 43:13165–13174